Original Article

Development of a novel tumor microenvironment-related radiogenomics model for prognosis prediction in hepatocellular carcinoma

Yaqi Wang[1], Bin Gao[1], Chunhua Xia[1], Xiaozheng Peng[2], Haifeng Liu[2], Senlin Wu[2]

[1]Department of Radiology, The Third Affiliated Hospital of Anhui Medical University (The First People's Hospital of Hefei), Hefei, China; [2]Department of Interventional Radiology, The Third Affiliated Hospital of Anhui Medical University (The First People's Hospital of Hefei), Hefei, China

Contributions: (I) Conception and design: Y Wang, B Gao; (II) Administrative support: B Gao, C Xia; (III) Provision of study materials or patients: Y Wang, H Liu, X Peng; (IV) Collection and assembly of data: Y Wang; (V) Data analysis and interpretation: Y Wang, H Liu, S Wu; (VI) Manuscript writing: All authors; (VII) Final approval of manuscript: All authors.

Correspondence to: Bin Gao, MD. Department of Radiology, The Third Affiliated Hospital of Anhui Medical University (The First People's Hospital of Hefei), 390 Huaihe Road, Hefei 230000, China. Email: gaobin_3136@163.com.

Background: The tumour microenvironment (TME) has occupied a potent position in the tumorigenesis and tumor progression of hepatocellular carcinoma (HCC). Radiogenomics is an emerging field that integrates imaging and genetic information, thus offering a novel class of non-invasive biomarkers with diagnostic, prognostic, and treatment response. However, optimal evaluation methodologies for radiogenomics in patients with HCC have not been well established. Therefore, this study aims to develop a radiogenomics models, associating contrast-enhanced computed tomography (CECT) based radiomics features and transcriptomics data with TME, to increase predictive precision for overall survival (OS) in patients with HCC.

Methods: Transcriptome profiles of 365 patients with HCC from The Cancer Genome Atlas (TCGA)-HCC cohort were used to obtain TME-related genes by differential expression analysis. TME-related radiomics features of 53 patients with HCC from The Cancer Imaging Archive (TCIA)-HCC cohort matched with the TCGA-HCC cohort were screened via correlation analysis. Furthermore, a radiogenomics score-based prognostic model was constructed using the least absolute shrinkage and selection operator (LASSO) Cox regression analysis in the TCIA-HCC cohort. Finally, the ability to predict prognosis and the value of the model in identifying the abundance of immune cell infiltration were investigated.

Results: A radiogenomics prognostic model was developed, which incorporated 1 radiomics feature [original_gray-level co-occurrence matrix (glcm)_inverse difference normalized (Idn)] and 3 genes [spen paralogue and orthologue C-terminal domain containing 1 (*SPOCD1*); killer cell lectin like receptor B1 (*KLRB1*); G protein-coupled receptor 182 (*GPR182*)]. The model performed satisfactorily in the training and test sets [1-year, 2-year, 3-year area under the curve (AUC) of 0.81, 0.85 and 0.87 in the training set, respectively; and 0.73, 0.83, and 0.84 in the test set, respectively]. Moreover, the model showed that higher radiogenomics scores were associated with worse OS and lower levels of immune infiltration.

Conclusions: The novel CECT-based radiogenomics model may provide valuable insights for prognostic stratification and TME assessment of patients with HCC.

Keywords: Hepatocellular carcinoma (HCC); computed tomography (CT); tumor microenvironment (TME); prognosis; radiogenomics

Submitted Aug 10, 2022. Accepted for publication Jul 14, 2023. Published online Aug 14, 2023.
doi: 10.21037/qims-22-840
View this article at: https://dx.doi.org/10.21037/qims-22-840

Introduction

Hepatocellular carcinoma (HCC), mainly a histological subtype of liver cancer, is currently the seventh most common malignancy and the second leading cause of cancer-related death worldwide (1). The long-term prognosis of patients with HCC still remains dismal (2). Molecular marker-based classification schemes for HCC have not been routinely applied, which greatly limits accurate treatment and prognosis prediction (3,4). Hence, it is essential to integrate multiomics factors for valuable biomarker acquisition, as this can provide a multidimensional basis for the selection of therapeutic options.

Accumulating research has highlighted the essential role of the tumor microenvironment (TME) in the progression of HCC (5-7). The TME is mainly composed of recruited immune cells and stromal cells that interact with cancer cells to promote the process of proliferation by resisting cell apoptosis and evading immune surveillance, ultimately affecting tumor metastasis, treatment effectiveness, and survival (6-8). In addition, the development of high-throughput genome sequencing technology in combination with genomics methods has clarified the characterization of the TME (6,9). Moreover, studies are gradually starting to focus on the novel field of radiogenomics, using genome-wide molecular data with high-throughput quantitative radiomics features to reveal the potential links with the genetic heterogeneity of tumors (10-12).

Thus far, only a limited number of studies have investigated the intratumoral heterogeneity distinction of clinical outcome in HCC (13-16), and a mature prognostic model based on radiogenomics method is lacking. Therefore, in this study, we aimed to develop a TME-related radiogenomics model derived from contrast-enhanced computed tomography (CECT) images for predicting prognosis and indicating the heterogeneity of TME in patients with HCC. We present this article in accordance with the TRIPOD reporting checklist (available at https://qims.amegroups.com/article/view/10.21037/qims-22-840/rc).

Methods

Patients

Clinical information and RNA-sequencing (RNA-seq) data of patients with HCC were downloaded from The Cancer Genome Atlas (TCGA; https://tcga-data.nci.nih.gov/tcga/). CT images of patients with HCC with matched RNA-seq data of TCGA-HCC cohort were obtained from The Cancer Imaging Archive (TCIA) (https://tcia.at/home/) and were randomly assigned to the training and test sets in a ratio of 1:1. All enrolled patients needed to be selected according to the exclusion criteria shown in *Figure 1*. These abovementioned data platforms are public and free of charge for scholars without ethical issues. The study was conducted in accordance with the Declaration of Helsinki (as revised in 2013).

Evaluation of TME with patients with HCC and acquisition of TME-related genes

The RNA-seq data of TCGA-HCC patients were used to score the abundance of ImmuneScore (Immune Component Ratio) and StromalScore (Matrix Component Ratio) with "ESTIMATE" package in R software 3.6.2 (https://www.r-project.org/). Co-up- and co-downregulated differentially expressed genes as TME-related genes were then obtained via differential expression analysis of the ImmuneSore and StromalScore groups with a threshold of $|\log_2\text{-fold change (FC)}| > 1$ and an adjusted P value <0.05 based on the median of ImmuneScore and StromalScore.

Extraction and selection of CT radiomics features

Since arterial-phase hypervascularity can better reflect the intratumoral heterogeneity, only the arterial phase of CECT images of the TCIA-HCC cohort with the standard scan parameters (tube voltage 120 KV, tube current 250 mA; matrix 512×512; thickness 1.5–3 mm; the arterial phase started 30–35 s after the injection, the venous phase started

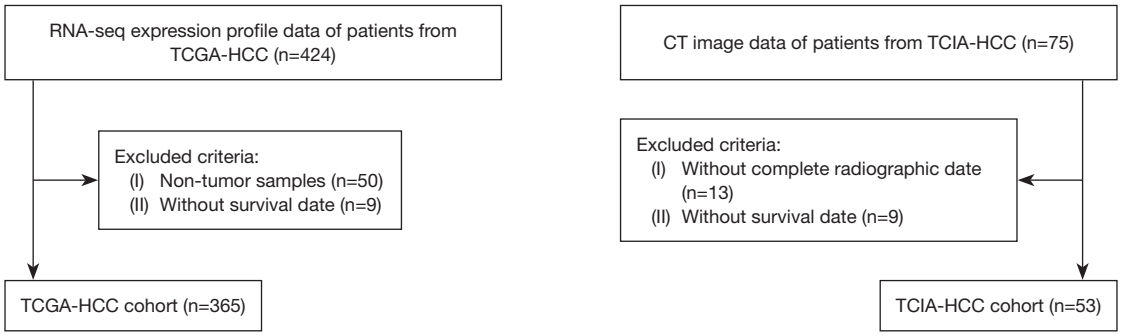

Figure 1 Flowchart of enrolled patients. RNA-seq, RNA sequencing; TCGA, The Cancer Genome Atlas; HCC, hepatocellular carcinoma; TCIA, The Cancer Imaging Archive.

after 55–60 s and the delayed phase started after 90–120 s) were imported into the open-source software 3D Slicer 4.10.2 (https://www.slicer.org/) for region of interest (ROI) acquisition. According to the standard of the Liver Reporting & Data System (LI-RADS) 2018 (17), a clearer tumor boundary on the portal venous phase images was defined as the delineation range, and two radiologists with at least 5 years of experience manually outlined the ROI of the entire tumor lesion on each slice. For cases of multiple lesions, the ROI was only delineated on the largest one. Two radiologists independently delineated all samples blindly without patient clinical information, then one of them repeated the ROI segmentation step. Prior to feature extraction, the image normalization process was performed by using the following specific parameter settings: a window level/width of 350/50 and a resampled pixel spacing of 1 mm × 1 mm × 3 mm. The image normalization and feature extraction steps were completed using the PyRadiomics package in Python 3.6 (https://python.org/). In total, 1,347 normalized radiomics features could be calculated according to following seven types of feature classes, including shape descriptors, first order, gray-level co-occurrence matrix (GLCM), gray-level run length matrix (GLRLM), gray-level size zone matrix (GLSZM), neighboring gray-tone difference matrix (NGTDM), and gray-level dependence matrix (GLDM), which were based on the original and eight filtered images types [Wavelet, Laplacian of Gaussian (LoG), Square, SquareRoot, Logarithm, Exponential, Gradient, and LocalBinaryPattern 2D/3D]. Subsequently, intra- and interclass correlation coefficient (ICC) analysis was used to select the stable and reproducible radiomics features (with Pearson correlation coefficient ICC ≥0.75 and P<0.05 being considered a strong correlation), which were further screened via Spearman correlation analysis using ImmuneScore and StromalScore.

Radiogenomics risk factor selection and prognostic model construction

First, in order to screen out prognosis-associated radiogenomics risk factors for model construction, univariate Cox regression analysis was performed for TME-related radiomics features and genes with survival data in TCGA-HCC and TCIA-HCC cohorts, respectively. Second, in the training set, a least absolute shrinkage and selection operator (LASSO) Cox regression analysis, a common machine learning method for feature selection, in combination with 10-fold cross-validation, was applied to select the most predictive features from outcomes of univariate Cox regression analysis. Subsequently, the radiogenomics score was calculated based on the following formula: $\beta_1 \times F_1 + \beta_2 \times F_2 + \beta_3 \times F_3 + \ldots$ (β is the LASSO Cox regression coefficient, and F is the value of the radiogenomics factors). This was taken as the radiogenomics prognostic prediction model. Additionally, we further verified the prognostic relevance of the genes in the radiogenomics score by multiple external independent cohorts (ICGC-HCC cohort: n=231; GSE10141 cohort: n=80; GSE54236 cohort: n=161; https://www.ncbi.nlm.nih.gov/geo/). Moreover, the relationship between radiogenomics score and clinical characteristics was analyzed.

Validation of the performance of the radiogenomics prognostic model

The area under the curve (AUC) of the time-dependent receiver operating characteristic (ROC) analyses was used

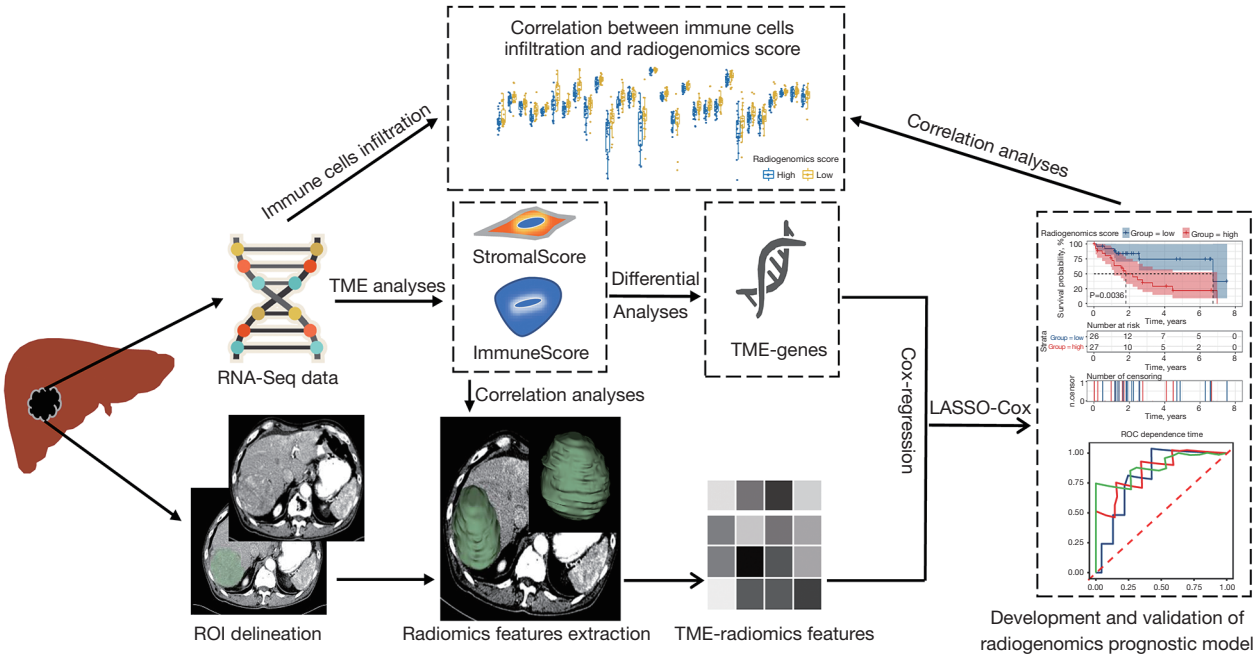

Figure 2 Analysis workflow of this study. RNA-Seq, RNA sequencing; ROI, region of interest; TME, tumor microenvironment; LASSO, least absolute shrinkage and selection operator; ROC, receiver operating characteristic.

to evaluate the predictive performance of the model with 1-, 2-, and 3-year overall survival (OS) in each of the training and test sets. Meanwhile, to maximize the clinical utility of the model, a quantifiable survival prediction probability nomogram was constructed based on the radiogenomics score in the training set. Calibration curves were plotted to obtain two sets of goodness of fit. The Kaplan-Meier (K-M) survival method was performed with log-rank test to determine whether there was a statistical difference in survival status between the high-risk and low-risk groups separated by the median radiogenomics score of each predictor in the TCIA-HCC cohort. Additionally, using single-sample gene set enrichment analysis (ssGSEA) method via the "GSVA" package in R, we calculated the abundance of immune cell infiltration, and the correlation with radiogenomics score was further confirmed by Spearman correlation analysis.

Statistical analysis

All statistical analysis, including differences analysis, ICC analysis, correlation analysis, survival analysis, regression analysis, and plots of Veen, volcano, time-dependent ROC curve, nomogram, and calibration curve were performed and graphed using R software, with significance defined as $P<0.05$.

Results

Patient clinical characteristics

The overall technical workflow is illustrated in *Figure 2*. There were a total of 365 patients with HCC from the TCGA datasets, and 53 patients with HCC with CECT images from the TCIA datasets. Enrolled patients from the TCIA-HCC cohort were randomly divided into a training set (n=27) and test set (n=26). The detailed clinical information of patients is presented in *Table 1* [pathological grading and clinical staging were determined according to the World Health Organization (WHO) classification system].

Identification of TME-related radiomics features and genes associated with prognosis

The result of the differential gene expression analysis in TCGA-HCC cohort was illustrated with volcano and Venn plots, with a total of 1,077 co-upregulated genes and 62 co-downregulated genes in the ImmuneScore and

Table 1 Clinical characteristics of patients with HCC in TCIA and TCGA cohort

Clinical factors	TCIA cohort (n=53)		TCGA cohort (n=365)
	Training set (n=27)	Test set (n=26)	
Age (years)			
≤65	15	13	228
>65	12	13	137
Gender			
Male	19	10	119
Female	8	16	246
Grade			
1	5	1	55
2	10	15	175
3	12	10	118
4	0	0	12
Unknown	0	0	5
Stage			
I	14	10	170
II	6	5	84
III	7	9	83
IV	0	2	4
Unknown	0	0	24
OS (days), median	667	475	596

HCC, hepatocellular carcinoma; TCIA, The Cancer Imaging Archive; TCGA, The Cancer Genome Atlas; OS, overall survival.

StromalScore groups ($|\log_2(FC)| > 1$ and adjusted P value <0.05) (*Figure 3A,3B*).

Meanwhile, for each patient in the TCIA-HCC cohort, 880 stable and reproducible radiomics features with ICCs >0.75 (P<0.05) were ultimately selected. After Spearman correlation analysis of each radiomics feature with ImmuneScore and StromalScore, 100 TME-related radiomics features were further screened (P<0.05; Figure S1).

Following the initial screening analysis described above, all the resulting TME-related radiomics features and differential genes were then used for univariate Cox regression analysis. Ultimately, 3 radiomics features and 20 genes (P<0.05) associated with prognosis remained, as demonstrated in the forest plot (*Figure 3C*).

Construction and validation of radiogenomics prognostic prediction model

In the LASSO Cox regression analysis, the radiogenomics prognostic prediction model was built in the training set using the 23 risk factors (3 radiomics features and 20 genes) obtained in the abovementioned analysis, and the optimal λ was chosen using internal 10-fold cross-validation, with 4 radiogenomics predictors with nonzero coefficients being identified (*Figure 3D*). Hence, a radiogenomics score-based OS prediction model calculated by a formula (radiogenomics score = 0.565 × original_glcm_Idn + 0.101 × SPOCD1 – 0.083 × KLRB1 – 1.221 × GPR182) was established (glcm, gray-level co-occurrence matrix; Idn, inverse difference normalized; SPOCD1, spen paralogue and orthologue C-terminal domain containing 1; KLRB1, killer cell lectin like receptor B1; GPR182, G protein-coupled receptor 182). Based on the TCIA-HCC cohort, higher OS-related radiogenomics scores were found for T3 than for T1 (P=0.017), and the same significant difference was observed between stage III and stage I (P=0.002), grade 3 and grade 1 (P=0.008), while no difference was observed for age, gender, or and N/M staging (Figure S2). In addition, multivariate logistic regression analysis demonstrated that TNM staging was an independent risk factor (Figure S3).

After construction of the prognostic model based on the training set, the AUCs of radiogenomics model were assessed at 1 year (AUC =0.81, cutoff =–0.13), 2 years (AUC =0.85, cutoff =–0.95), and 3 years (AUC =0.87, cutoff =–1.13) in the training set, and 1 year (AUC =0.73), 2 years (AUC =0.83), and 3 years (AUC =0.84) in the test set, suggesting a good predictive ability of the model (*Figure 4A*). The radiogenomics model had a superior AUC to the model using only TNM staging (Figure S3). To present the predictive model, a nomogram was constructed to facilitate its widespread use by researchers (*Figure 4B*). Furthermore, all patients in the TCIA-HCC cohort were classified the high- or low-score group according to the median radiogenomics score of the training set (–0.378), and the K-M survival curve was plotted to demonstrate the significant difference in OS between two groups [hazard ratio (HR) =3.631, 95% CI =1.437–9.177; log-rank test P=0.0036] (*Figure 4C*). The K-M survival curve and OS status distribution intuitively revealed a worse OS in patients with higher radiogenomics scores (*Figure 4D*). Moreover, K-M survival analysis was performed for four predictors as well (Figure S4). Additionally, validation of three external independent cohorts further

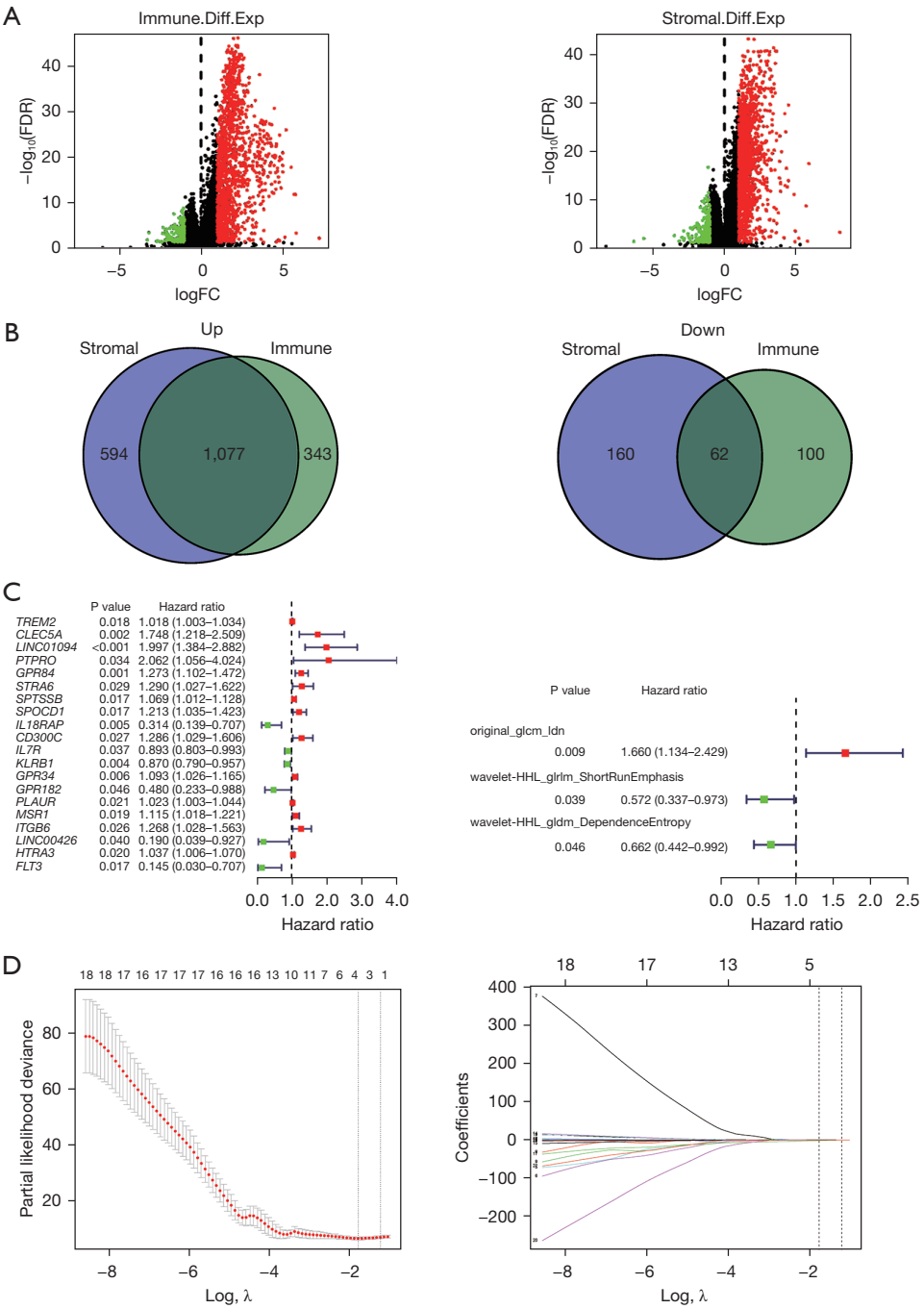

Figure 3 TME-related radiogenomics risk factor selection for prognostic model construction. (A) Volcano plots for the differential express genes of ImmuneScore (left) and StromalScore (right) determined by threshold of $|\log_2(FC)| > 1$ with an adjusted P value <0.05 in the TCGA-HCC cohort. The red dots indicate upregulated genes with an adjusted P value <0.05. The green dots indicate downregulated genes with an adjusted P value <0.05. The black dots indicate genes with no significant differential expression (adjusted P value >0.05). (B) Venn plots showing co-upregulated (left) and co-downregulated (right) genes of ImmuneScore and StromalScore. (C) Forest plots for the univariate Cox regression analysis with TME-related differential genes (left) and radiomics features (right) in TCGA and TCIA cohorts, with the significant factors with P<0.05 being listed. (D) Optimal λ selection according to 10-fold cross-validation (left) and LASSO coefficient profiles of all radiogenomics risk factors (right) in the training set. FDR, false discovery rate; Diff., difference; Exp, expression; FC, fold change; TME, tumor microenvironment; TCGA, The Cancer Genome Atlas; HCC, hepatocellular carcinoma; TCIA, The Cancer Imaging Archive; LASSO, least absolute shrinkage and selection operator.

confirmed the prognostic relevance of the three genes in the radiogenomics score (Figure S5). Finally, the reliability of the model for prediction at different time points was observed via calibration curves, which showed that the longer the survival time was, the better the calibration of the model (Figure S6). Comparing the prognosis prediction performance of the 3-gene classifier and the radiomics feature in the model, we found that the value of gene-based prognosis prediction mainly reflected the short-term prognosis, while radiomics features showed significant advantages in long-term outcomes (Figure S7).

Correlation of radiogenomics score with TME

As all patients in the TCGA-HCC cohort with 29 tumor-infiltrating immune cell enrichment scores were quantified via the ssGSEA method (Figure S8), we analyzed the association between the radiogenomics score and abundance of immune cells infiltration in TCIA-HCC cohort. Our results showed that the infiltration abundance of 22 kinds of immune cells was significantly different between the high and low radiogenomics score groups (P<0.05) (*Figure 5*), of which 21 were negatively correlated with the score (P<0.05) (Figure S9).

Discussion

In our study, we investigated the correlation between the heterogeneity of TME and prognosis in patients with HCC and whether it could be used as a biomarker based on radiogenomics analysis to develop an effective quantitative model for predicting prognosis. For this purpose, we identified four predictors (original_glcm_Idn, SPOCD1, KLRB1, and GPR182) and established a quantitative prediction model that performed satisfactorily in the training and testing sets. Moreover, the radiogenomics score based on the above four prognostic predictors could well reflect the heterogeneity of the TME in patients with HCC, especially the infiltration abundance of immune cells.

Thus far, a number of staging systems have been used to evaluate the prognosis of patients with HCC and to guide the choice of treatment, such as Barcelona clinic liver cancer (BCLC) staging, The Hong Kong liver cancer (HKLC) staging, Cancer of the Liver Italian Program (CLIP) grading, and the eight edition TNM stage system, but these have shown limited effectiveness in reflecting the internal heterogeneity and molecular characteristics of the tumor at a macroscopic scale (18). Through the fusion of the noninvasive and repeatable high-dimensional imaging information and the gene sequencing data, radiogenomics has been considered as a potential biological marker for revealing the molecular function of whole tumor morphology and has proven capable in the evaluation of tumor efficacy, prognosis, and expanding the understanding of tumor biological mechanism.

A series of previous studies has examined the application of radiogenomics in a variety of tumors, but this is rare in HCC (12,19-21). Segal *et al.* (22), first reported a combination of various quantitative radiomics features extracted from three phase enhanced CT images of patients with HCC, which allowed the reconstruction of 80% of the global gene expression profile, demonstrating a correlation with cell proliferation, liver synthesis function, and prognosis relevance. Subsequently, most studies have focused on the relationship between radiomics and clinical features or tumor heterogeneity, few of which have developed stable predictive models (23-26). A CECT-based radiomics model achieved a satisfactory prediction result in predicting microvascular infiltration of HCC (AUC =0.72 in test set) and provided a new approach for TME and tumor heterogeneity (26). In addition, a radiomics model for recurrence risk prediction was developed from a multi-institutional study, which exhibited better prognostic power than did other staging systems (test set AUC: 0.84–0.88 *vs.* 0.58–0.60) and successfully divided patients with HCC into three recurrence risk subgroups (23). Moreover, in order to find an effective method to identify patients with HCC who might respond to immunotherapy, Liao *et al.* (27) constructed a radiomics model based on CECT to predict the immune infiltration of $CD8^+$ T cells in HCC (AUC =0.705 in test set). Another clinical-radiomics model was established using CECT images which demonstrated superior performance in predicting the response to first transcatheter arterial chemoembolization (TACE) treatment in patients with intermediate-stage HCC (28).

In contrast, radiogenomics analysis of HCC has thus far been limited. Among the single literature reports that we are aware of, some researchers observed that multiple conventional imaging traits were correlated with the key genes related to the HCC phenotype (11,12). In another recent paper, a model based on the radiomic signature extracted from volume of interest covering 10 mm from the tumor margin (VOI_{10mm}) in the arterial phase demonstrated the highest AUC (0.733), compared to the VOI_{5mm} (AUC =0.679) and VOI_{20mm} (AUC =0.719), for characterizing alterations of PI3K signaling in HCC (19). Drawing on

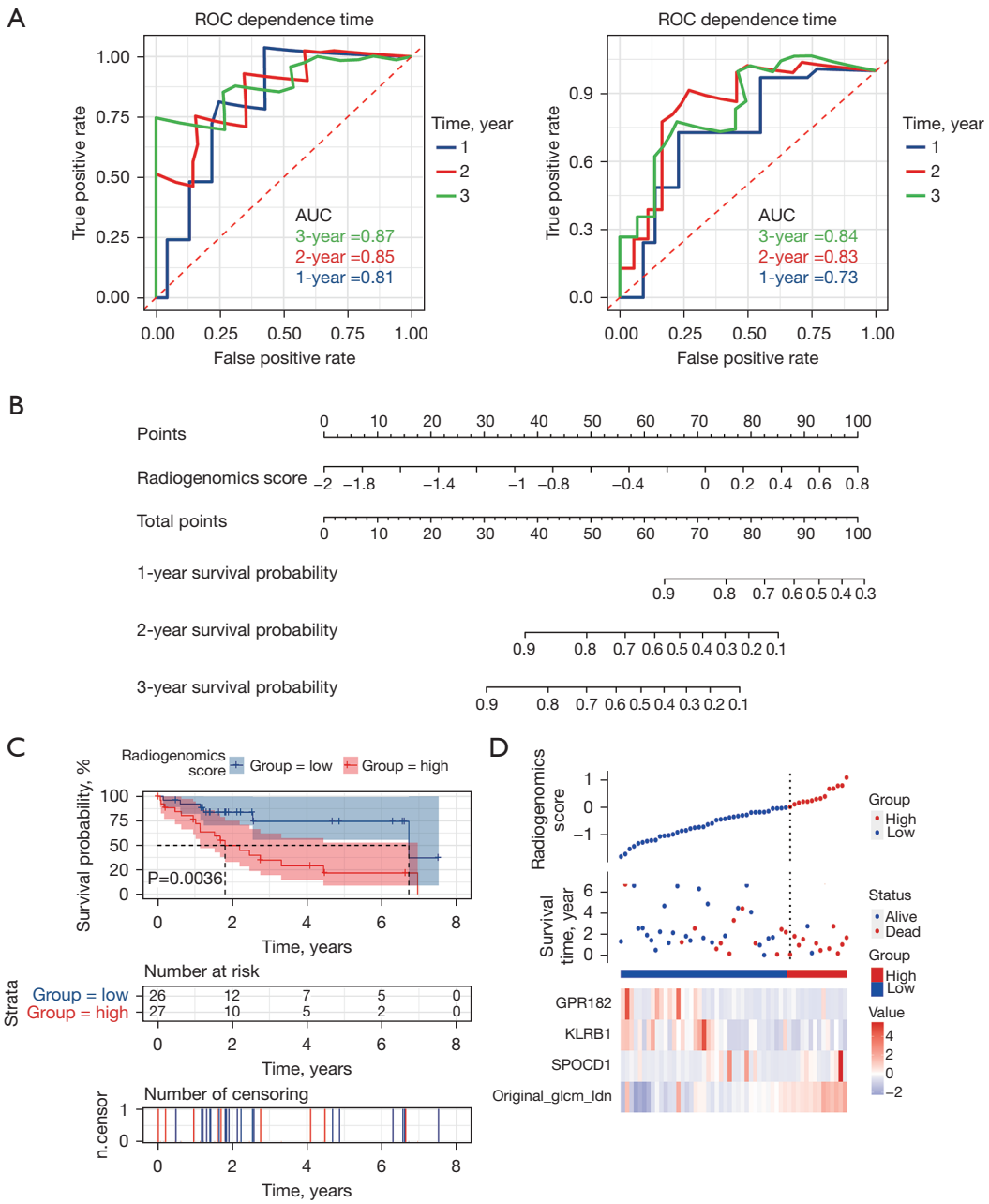

Figure 4 Performance of the radiogenomics prognostic model. (A) Time-dependent ROC curves for 1-, 2-, 3-year OS prediction in the training (left) and test set (right). (B) The nomogram was constructed with the radiogenomics score for predicting the OS of patients with HCC. (C) The Kaplan-Meier curve for patients with high and low radiogenomics score. (D) Distribution of radiogenomics score with survival data and heatmap depiction of 4 predictors in the model. ROC, receiver operating characteristic; AUC, area under curve; OS, overall survival; HCC, hepatocellular carcinoma.

the research experience of previous studies in the field of radiogenomics, we combined RNA-seq data with radiomics parameters of HCC to develop 4 prognostic predictors reflecting intratumoral heterogeneity. The inverse difference normalized (IDN) of GLCM was characterized as a measure of a local homogeneity of the images, with higher values being associated with more homogeneous different regions of image texture, which has been reported

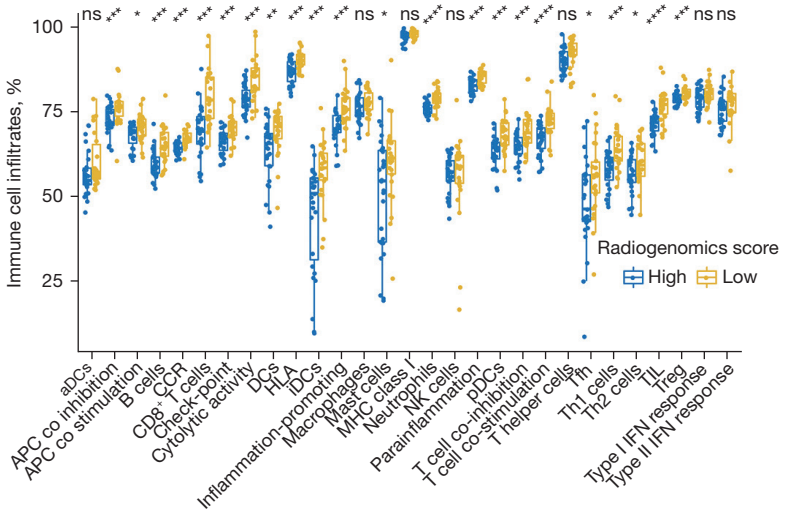

Figure 5 Correlation of tumor-infiltrating immune cells with radiogenomics score. Box plots showed the ratio differentiation of 29 kinds of immune cells between patients with HCC with a high and low radiogenomics score. The statistical difference was compared with the Wilcoxon test: *, P<0.05; **, P<0.01; ***, P<0.001; ****, P<0.0001; ns, P>0.05. ns, not significant; HCC, hepatocellular carcinoma; aDCs, activated dendritic cells; APC, antigen presenting cells; CCR, chemokines receptor; CD, cluster of differentiation; DCs, activated dendritic cells; HAL, human leukocyte antigen; iDCs immature dendritic cells; MHC, major histocompatibility complex; NK, natural killer; pDCs, plasmacytoid dendritic cells; Tfh, follicular helper T cell; Th, T helper cell; TIL, tumor infiltrating lymphocytes; Treg, regulatory T cells; IFN, interferon.

in other studies to reflect the heterogeneity of the tumor (29,30). In this study, original_glcm_Idn was negatively correlated with ImmuneScore and StromalScore. This may imply that higher image heterogeneity is associated with lower level immune infiltration, both of which may collectively indicated poor prognosis. In a recent study, the $CD8^+$ T cells characterized by high expression of KLRB1 in early-relapse HCC showed lower cytotoxicity and immunosuppression in contrast to the depleted state found in primary HCC (6). Furthermore, a study identified that GPR182 was a negative regulator of intestinal mitogen-activated protein kinase (MAPK) signal-induced proliferation, which might lead to further emergence adenoma and reduced survival (31). Other studies have found that SPOCD1 could promote the proliferation and metastasis of tumor cells and was correlated with poor prognosis (32,33). It should be further mentioned that the differential expression of the three prognosis-related genes mentioned above resulted in significant differences in patient prognosis of between 0 and 2.5 years but with poor ability to stratify patient prognosis in the long-term. However, the radiomics feature can better reflect the difference in the long-term prognosis. Because of the spatial heterogeneity of tumors stemming from the heterogeneity of TME and the random nature of gene mutations, only a subset of pathological features can be understood based on individual biopsies, making it difficult for these genes to reflect the overall distribution of immune infiltration that has hindered the assessment of patient prognosis (34,35). However, radiomics features we extracted based on the entire lesion range, which may better reflect spatial heterogeneity and provide more comprehensive tumor molecular and pathological information and could be used as an imaging biomarker with additional prognostic predictive value for patients.

Some limitations to this study should be mentioned. First, the sample size was small, especially for patients available for radiological follow-up, while the number of external multicenter cohorts was insufficient for verifying the reliability of the predictive factors. Second, the abundance of immune cells in tumor tissue remains to be experimentally addressed. Third, the perinodular region of lesions was not included in the ROIs, so the potentially valuable radiographic information with intratumor heterogeneity of this region should be further investigated.

Conclusions

We developed a new prognostic model containing four

radiogenomics predictors associated with TME that showed good performance in determining the prognosis of patients with HCC and different immune infiltrates. Findings from this study can be expected to provide a reliable reference for decision-making in clinical practice.

Acknowledgments

The authors would like to thank the TCGA, ICGC, TCIA, and Gene Expression Omnibus for database access.
Funding: None.

Footnote

Reporting Checklist: The authors have completed the TRIPOD reporting checklist. Available at https://qims.amegroups.com/article/view/10.21037/qims-22-840/rc

Conflicts of Interest: All authors have completed the ICMJE uniform disclosure form (available at https://qims.amegroups.com/article/view/10.21037/qims-22-840/coif). The authors have no conflicts of interest to declare.

Ethical Statement: The authors are accountable for all aspects of the work in ensuring that questions related to the accuracy or integrity of any part of the work are appropriately investigated and resolved. The study was conducted in accordance with the Declaration of Helsinki (as revised in 2013). Institutional review board approval and informed consent were not required because all patients' data included in this study are publicly and freely available for scientific study purposes.

References

1. Siegel RL, Miller KD, Fuchs HE, Jemal A. Cancer statistics, 2022. CA Cancer J Clin 2022;72:7-33.
2. Zhu P, Liao W, Zhang WG, Chen L, Shu C, Zhang ZW, Huang ZY, Chen YF, Lau WY, Zhang BX, Chen XP. A Prospective Study Using Propensity Score Matching to Compare Long-term Survival Outcomes After Robotic-assisted, Laparoscopic, or Open Liver Resection for Patients With BCLC Stage 0-A Hepatocellular Carcinoma. Ann Surg 2023;277:e103-11.
3. Bahcivanci B, Shafiha R, Gkoutos GV, Acharjee A. Associating transcriptomics data with inflammatory markers to understand tumour microenvironment in hepatocellular carcinoma. Cancer Med 2023;12:696-711.
4. Huo J, Cai J, Wu L. Comprehensive analysis of metabolic pathway activity subtypes derived prognostic signature in hepatocellular carcinoma. Cancer Med 2023;12:898-912.
5. Al-Shawi AAA, El-Arabey AA, Mutlaq DZ, Eltayb WA, Iriti M, Abdalla M. Study on Molecular Anti-tumor Mechanism of 2-Thiohydantoin Derivative based on Molecular Docking and Bioinformatic Analyses. Curr Top Med Chem 2023;23:440-52.
6. Sun Y, Wu L, Zhong Y, Zhou K, Hou Y, Wang Z, et al. Single-cell landscape of the ecosystem in early-relapse hepatocellular carcinoma. Cell 2021;184:404-421.e16.
7. Zheng C, Zheng L, Yoo JK, Guo H, Zhang Y, Guo X, Kang B, Hu R, Huang JY, Zhang Q, Liu Z, Dong M, Hu X, Ouyang W, Peng J, Zhang Z. Landscape of Infiltrating T Cells in Liver Cancer Revealed by Single-Cell Sequencing. Cell 2017;169:1342-1356.e16.
8. Murai H, Kodama T, Maesaka K, Tange S, Motooka D, Suzuki Y, et al. Multiomics identifies the link between intratumor steatosis and the exhausted tumor immune microenvironment in hepatocellular carcinoma. Hepatology 2023;77:77-91.
9. Yin Z, Ma T, Chen S, Yu M. Identification of therapeutic targets and prognostic biomarkers among CXC chemokines in hepatocellular carcinoma microenvironment. Cancer Biomark 2023;36:231-50.
10. Dai H, Lu M, Huang B, Tang M, Pang T, Liao B, Cai H, Huang M, Zhou Y, Chen X, Ding H, Feng ST. Considerable effects of imaging sequences, feature extraction, feature selection, and classifiers on radiomics-based prediction of microvascular invasion in hepatocellular carcinoma using magnetic resonance imaging. Quant Imaging Med Surg 2021;11:1836-53.
11. Chong H, Gong Y, Zhang Y, Dai Y, Sheng R, Zeng M. Radiomics on Gadoxetate Disodium-enhanced MRI: Non-invasively Identifying Glypican 3-Positive Hepatocellular Carcinoma and Postoperative Recurrence. Acad Radiol 2023;30:49-63.
12. An J, Oh M, Kim SY, Oh YJ, Oh B, Oh JH, Kim W, Jung

JH, Kim HI, Kim JS, Sung CO, Shim JH. PET-Based Radiogenomics Supports mTOR Pathway Targeting for Hepatocellular Carcinoma. Clin Cancer Res 2022;28:1821-31.
13. Piñero F, Dirchwolf M, Pessôa MG. Biomarkers in Hepatocellular Carcinoma: Diagnosis, Prognosis and Treatment Response Assessment. Cells 2020;9:1370.
14. Lewin M, Laurent-Bellue A, Desterke C, Radu A, Feghali JA, Farah J, Agostini H, Nault JC, Vibert E, Guettier C. Evaluation of perfusion CT and dual-energy CT for predicting microvascular invasion of hepatocellular carcinoma. Abdom Radiol (NY) 2022;47:2115-27.
15. Feng Z, Li H, Liu Q, Duan J, Zhou W, Yu X, Chen Q, Liu Z, Wang W, Rong P. CT Radiomics to Predict Macrotrabecular-Massive Subtype and Immune Status in Hepatocellular Carcinoma. Radiology 2023;307:e221291.
16. Liao H, Xiong T, Peng J, Xu L, Liao M, Zhang Z, Wu Z, Yuan K, Zeng Y. Classification and Prognosis Prediction from Histopathological Images of Hepatocellular Carcinoma by a Fully Automated Pipeline Based on Machine Learning. Ann Surg Oncol 2020;27:2359-69.
17. Chernyak V, Fowler KJ, Kamaya A, Kielar AZ, Elsayes KM, Bashir MR, Kono Y, Do RK, Mitchell DG, Singal AG, Tang A, Sirlin CB. Liver Imaging Reporting and Data System (LI-RADS) Version 2018: Imaging of Hepatocellular Carcinoma in At-Risk Patients. Radiology 2018;289:816-30.
18. Yu Y, Fan Y, Wang X, Zhu M, Hu M, Shi C, Hu C. Gd-EOB-DTPA-enhanced MRI radiomics to predict vessels encapsulating tumor clusters (VETC) and patient prognosis in hepatocellular carcinoma. Eur Radiol 2022;32:959-70.
19. Liao H, Jiang H, Chen Y, Duan T, Yang T, Han M, Xue Z, Shi F, Yuan K, Bashir MR, Shen D, Song B, Zeng Y. Predicting Genomic Alterations of Phosphatidylinositol-3 Kinase Signaling in Hepatocellular Carcinoma: A Radiogenomics Study Based on Next-Generation Sequencing and Contrast-Enhanced CT. Ann Surg Oncol 2022. [Epub ahead of print]. doi: 10.1245/s10434-022-11505-4.
20. Wu H, Wu C, Zheng H, Wang L, Guan W, Duan S, Wang D. Radiogenomics of neuroblastoma in pediatric patients: CT-based radiomics signature in predicting MYCN amplification. Eur Radiol 2021;31:3080-9.
21. Moussa AM, Ziv E. Radiogenomics in Interventional Oncology. Curr Oncol Rep 2021;23:9.
22. Segal E, Sirlin CB, Ooi C, Adler AS, Gollub J, Chen X, Chan BK, Matcuk GR, Barry CT, Chang HY, Kuo MD. Decoding global gene expression programs in liver cancer by noninvasive imaging. Nat Biotechnol 2007;25:675-80.
23. Ji GW, Zhu FP, Xu Q, Wang K, Wu MY, Tang WW, Li XC, Wang XH. Machine-learning analysis of contrast-enhanced CT radiomics predicts recurrence of hepatocellular carcinoma after resection: A multi-institutional study. EBioMedicine 2019;50:156-65.
24. Cui H, Zeng L, Li R, Li Q, Hong C, Zhu H, Chen L, Liu L, Zou X, Xiao L. Radiomics signature based on CECT for non-invasive prediction of response to anti-PD-1 therapy in patients with hepatocellular carcinoma. Clin Radiol 2023;78:e37-44.
25. Jiang C, Zhao L, Xin B, Ma G, Wang X, Song S. (18) F-FDG PET/CT radiomic analysis for classifying and predicting microvascular invasion in hepatocellular carcinoma and intrahepatic cholangiocarcinoma. Quant Imaging Med Surg 2022;12:4135-50.
26. Xia TY, Zhou ZH, Meng XP, Zha JH, Yu Q, Wang WL, Song Y, Wang YC, Tang TY, Xu J, Zhang T, Long XY, Liang Y, Xiao WB, Ju SH. Predicting Microvascular Invasion in Hepatocellular Carcinoma Using CT-based Radiomics Model. Radiology 2023;307:e222729.
27. Liao H, Zhang Z, Chen J, Liao M, Xu L, Wu Z, Yuan K, Song B, Zeng Y. Preoperative Radiomic Approach to Evaluate Tumor-Infiltrating CD8(+) T Cells in Hepatocellular Carcinoma Patients Using Contrast-Enhanced Computed Tomography. Ann Surg Oncol 2019;26:4537-47.
28. Schobert IT, Savic LJ, Chapiro J, Bousabarah K, Chen E, Laage-Gaupp F, Tefera J, Nezami N, Lin M, Pollak J, Schlachter T. Neutrophil-to-lymphocyte and platelet-to-lymphocyte ratios as predictors of tumor response in hepatocellular carcinoma after DEB-TACE. Eur Radiol 2020;30:5663-73.
29. Yu L, Tao G, Zhu L, Wang G, Li Z, Ye J, Chen Q. Prediction of pathologic stage in non-small cell lung cancer using machine learning algorithm based on CT image feature analysis. BMC Cancer 2019;19:464.
30. Ghosh A, Malla SR, Bhalla AS, Manchanda S, Kandasamy D, Kumar R. Texture analysis of routine T2 weighted fat-saturated images can identify head and neck paragangliomas - A pilot study. Eur J Radiol Open 2020;7:100248.
31. Kechele DO, Blue RE, Zwarycz B, Espenschied ST, Mah AT, Siegel MB, Perou CM, Ding S, Magness ST, Lund PK, Caron KM. Orphan Gpr182 suppresses ERK-mediated intestinal proliferation during regeneration and

adenoma formation. J Clin Invest 2017;127:593-607.
32. Liu Q, Wang XY, Qin YY, Yan XL, Chen HM, Huang QD, Chen JK, Zheng JM. SPOCD1 promotes the proliferation and metastasis of glioma cells by up-regulating PTX3. Am J Cancer Res 2018;8:624-35.
33. Wang C, Wang J, Shen X, Li M, Yue Y, Cheng X, Lu W, Wang X, Xie X. LncRNA SPOCD1-AS from ovarian cancer extracellular vesicles remodels mesothelial cells to promote peritoneal metastasis via interacting with G3BP1. J Exp Clin Cancer Res 2021;40:101.
34. Sun YF, Wu L, Liu SP, Jiang MM, Hu B, Zhou KQ, et al. Dissecting spatial heterogeneity and the immune-evasion mechanism of CTCs by single-cell RNA-seq in hepatocellular carcinoma. Nat Commun 2021;12:4091.
35. Nguyen PHD, Ma S, Phua CZJ, Kaya NA, Lai HLH, Lim CJ, et al. Intratumoural immune heterogeneity as a hallmark of tumour evolution and progression in hepatocellular carcinoma. Nat Commun 2021;12:227.

Cite this article as: Wang Y, Gao B, Xia C, Peng X, Liu H, Wu S. Development of a novel tumor microenvironment-related radiogenomics model for prognosis prediction in hepatocellular carcinoma. Quant Imaging Med Surg 2023;13(9):5803-5814. doi: 10.21037/qims-22-840

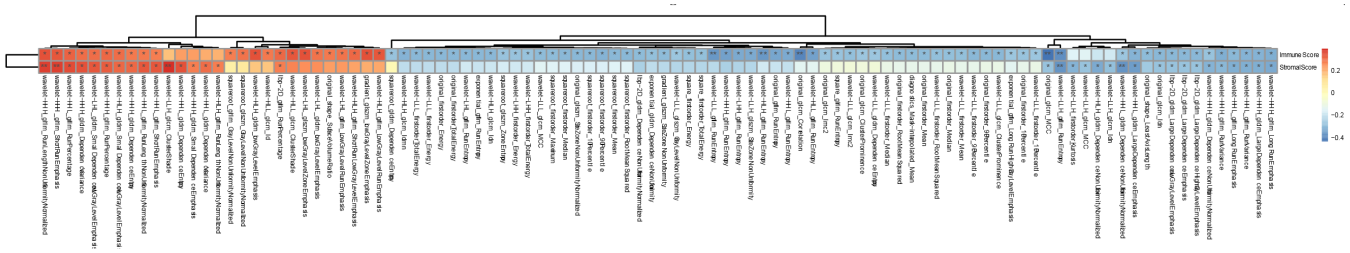

Figure S1 Heatmap of TME-related radiomics features. Heatmap showing the 100 TME-related radiomics features selected by non-parametric Spearman correlation analysis with ImmuneScore and StromalScore (P<0.05). TME, tumor microenvironment.

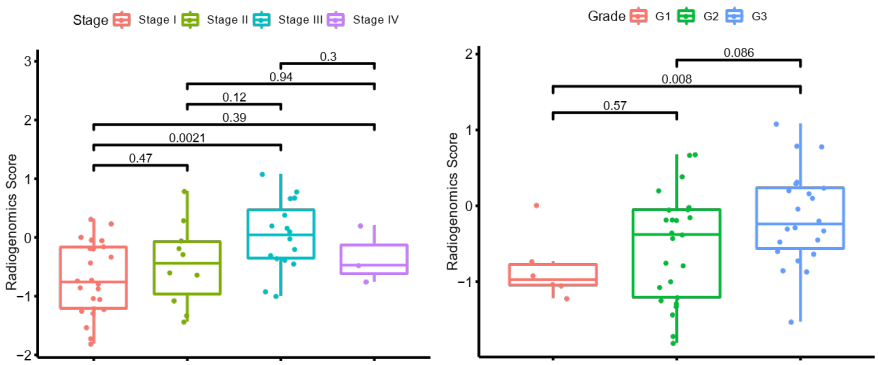

Figure S2 Analysis of correlation between radiogenomics score and clinical characteristics. Box-plots showing significant difference in the radiogenomics score between stage I and stage III (left), and between grade 1 and grade 3 (right). The differences were compared through the Wilcoxon test.

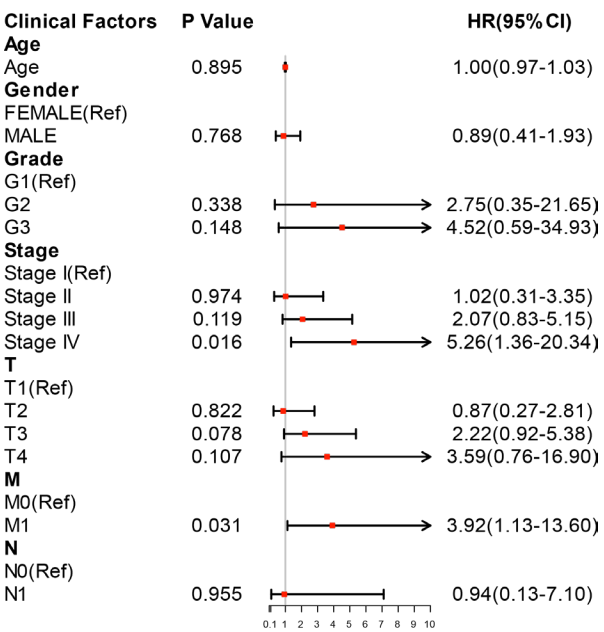

https://dx.doi.org/10.21037/qims-22-840

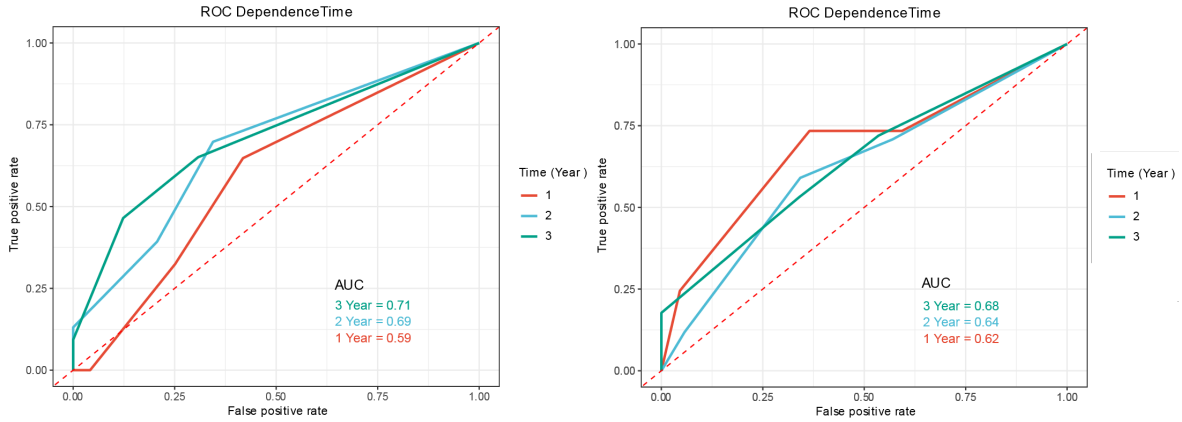

Figure S3 Multivariate Cox regression analysis for clinical factors. To evaluate the independent prediction performance of the clinical factors, multivariate Cox regression analyses were conducted on the TCGA-HCC cohort (n=365) and demonstrated that TNM staging was independent risk factor. ROC curves were plotted based on TNM staging in the training cohort (left) the test cohort (right). TCGA, The Cancer Genome Atlas; HCC, hepatocellular carcinoma; ROC, receiver operating characteristic; AUC, area under the curve.

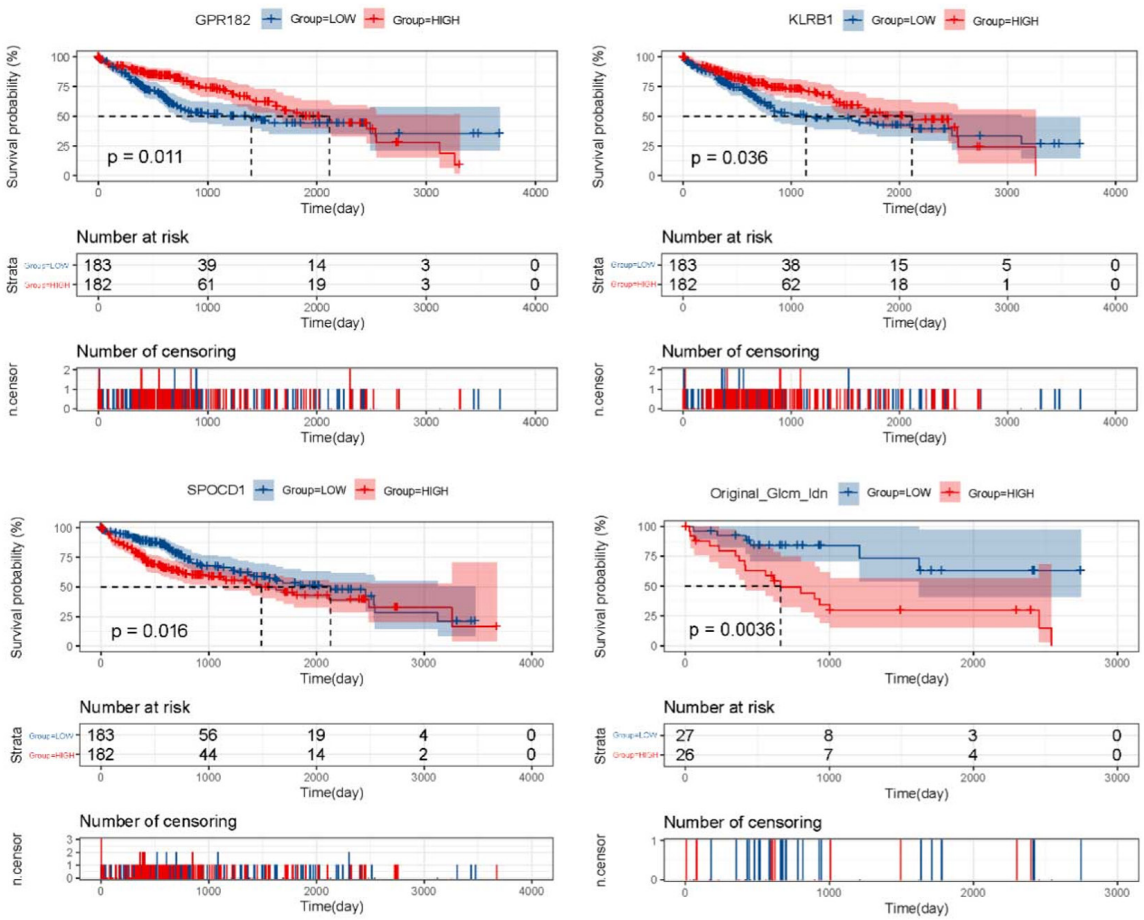

Figure S4 Survival analysis of four radiogenomics predictors. Survival analysis using the Kaplan-Meier method according to high (above the median) and low (below the median) expression of 3 genes (*GPR182*, *KLRB1*, and *SPOCD1*) in TCGA-HCC cohort and value of a radiomics feature (Original_Glcm_Idn) in TCIA-HCC cohort. TCGA, The Cancer Genome Atlas; HCC, hepatocellular carcinoma; TCIA, The Cancer Imaging Archive.

https://dx.doi.org/10.21037/qims-22-840

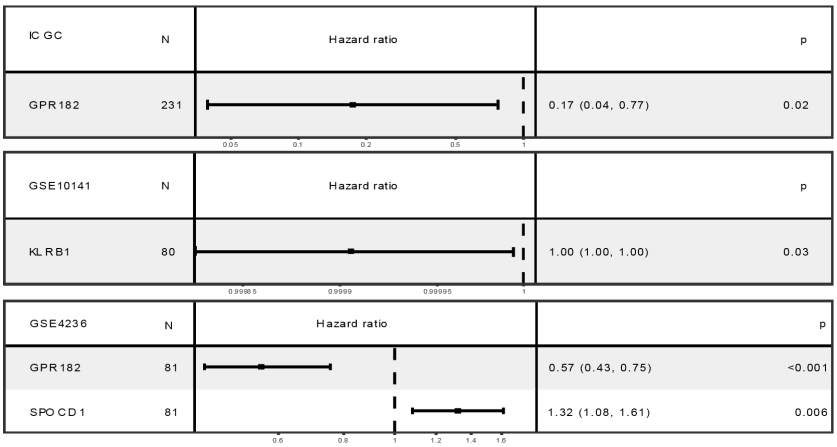

Figure S5 Verification of prognostic genes of the model in other three test sets. Three prognostic genes of the model were further validated by other three sets of validation datasets (ICGC, GSE10141 and GSE4236).

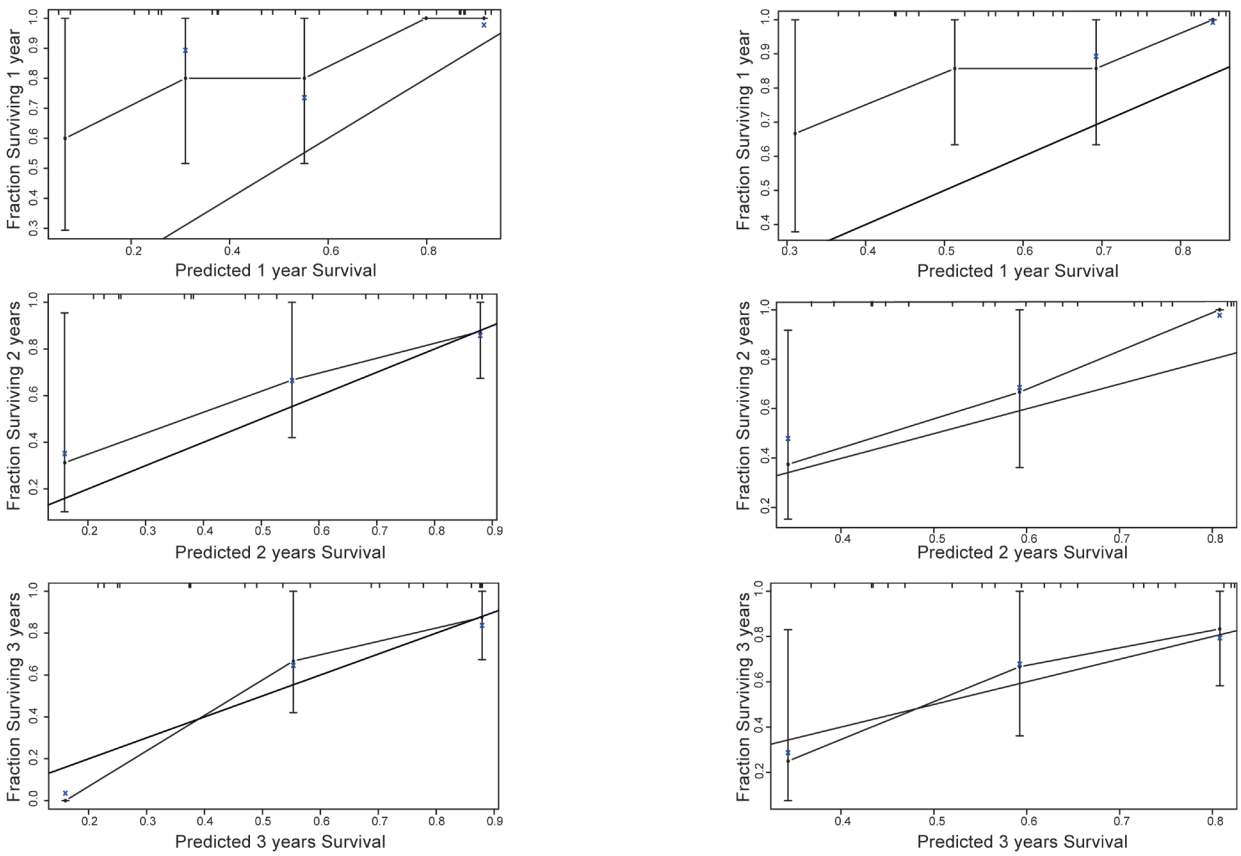

Figure S6 Calibration curve of prediction model in training set and test set. The 1-, 2- and 3-year calibration plots of prediction model in the training cohort (left) the test cohort (right). (Cmethod="KM", Method="boot", B=100, Hosmer-Lemeshow test: P>0.05).

https://dx.doi.org/10.21037/qims-22-840

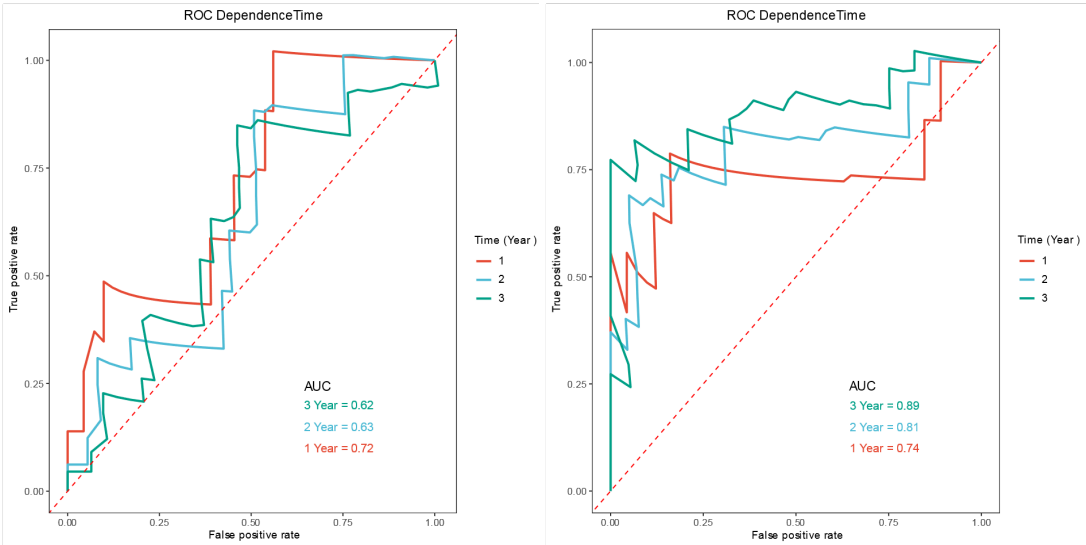

Figure S7 Based on the entire dataset (TCIA-HCC, n=53), ROC curves of 3-gene classifier (left) and 1 radiomics feature (original_glcm_Idn) (right) in the radiogenomics model for prognosis prediction. TCIA, The Cancer Imaging Archive; HCC, hepatocellular carcinoma; ROC, receiver operating characteristic; AUC, area under the curve.

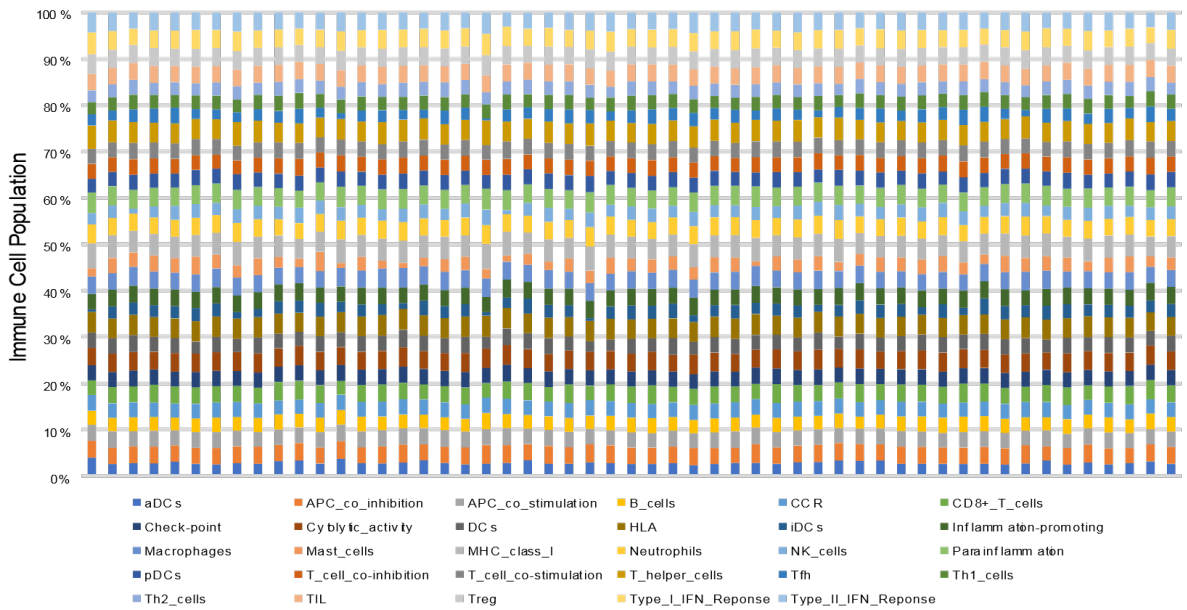

Figure S8 Proportion of tumor-infiltrating immune cells in TCIA-HCC cohort. Barplot showing the proportion of 29 kinds of tumor-infiltrating immune cells in TCIA-HCC cohort. TCIA, The Cancer Imaging Archive; HCC, hepatocellular carcinoma

https://dx.doi.org/10.21037/qims-22-840

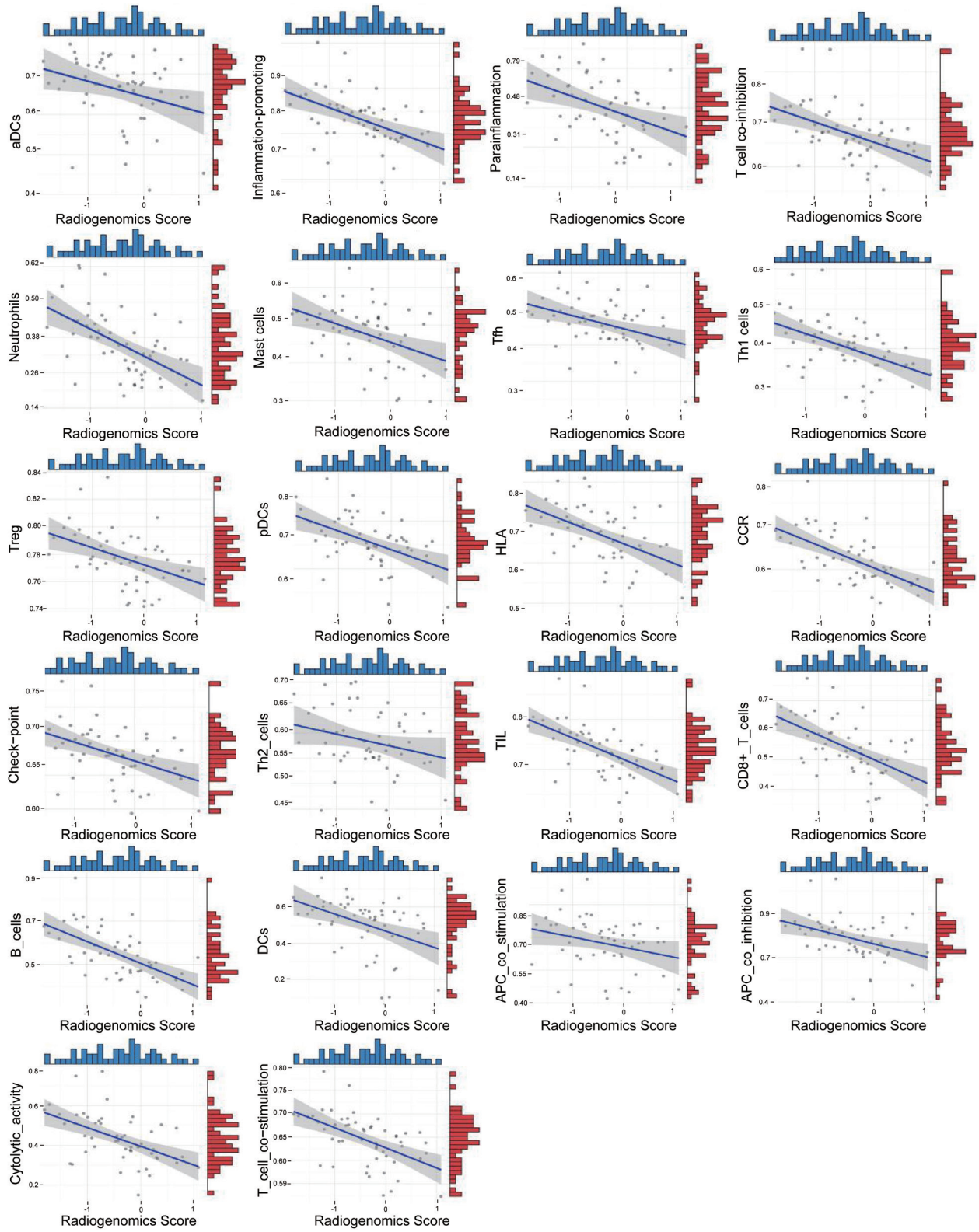

Figure S9 Analysis of correlation between radiogenomics score and tumor-infiltrating immune cells. Scatter plot showed the correlation of 22 kinds of tumor-infiltrating immune cells with the radiogenomics score and Spearman coefficient was used for the correlation test.

https://dx.doi.org/10.21037/qims-22-840